

## A metamaterial combining electric- and magnetic- dipole-based configurations for unique dual-band signal enhancement in ultra-high field magnetic resonance imaging

Rita Schmidt<sup>1,2\*</sup> and Andrew Webb<sup>1</sup>

<sup>1</sup>Department of Radiology, Leiden University Medical Center, Leiden, Netherlands

<sup>2</sup>Visiting Scientist in Department of Neurobiology, Weizmann Institute of Science, Rehovot, Israel

E-mail: rita.schmidt@weizmann.ac.il

### S1. Zigzag-shaped versus straight-line strips metamaterial

The metasurface, comprising of a set of conducting strips added to a dielectric substrate, supports a set of electromagnetic modes generated by a system of electric dipoles. For  $N$  strips,  $N-1$  modes with different penetration depths into the sample are generated. For MRI purposes we chose the most penetrating mode. The frequency of the mode depends primarily on the length of the copper strips. In the current work, we aimed to reduce the metamaterial's dimensions by utilizing zigzag-shape copper strips instead of straight-line strips. The zigzag-shape enables the electric dipole to be extended to the length required by the desired resonant frequency while minimizing the physical dimensions of the pad. Figures S1a,b show the spatial distribution of the H-field, comparing zigzag-shaped and straight-line strips designed for the  $^{31}\text{P}$  frequency at 7 T (121.7 MHz). In addition to the H-field distribution, we also examined the E-field distribution, since it produces power deposition (defined by the specific absorption rate (SAR)) in the sample. The simulation showed that the maximum value of the E-field for the same H-field is 7% less for S1a versus S1b. The reduction in setup dimensions and local maximum E-field can be even more substantial for applications at lower frequencies, for example for  $^1\text{H}$  at 1.5 T or other heteronuclei such as carbon or sodium.

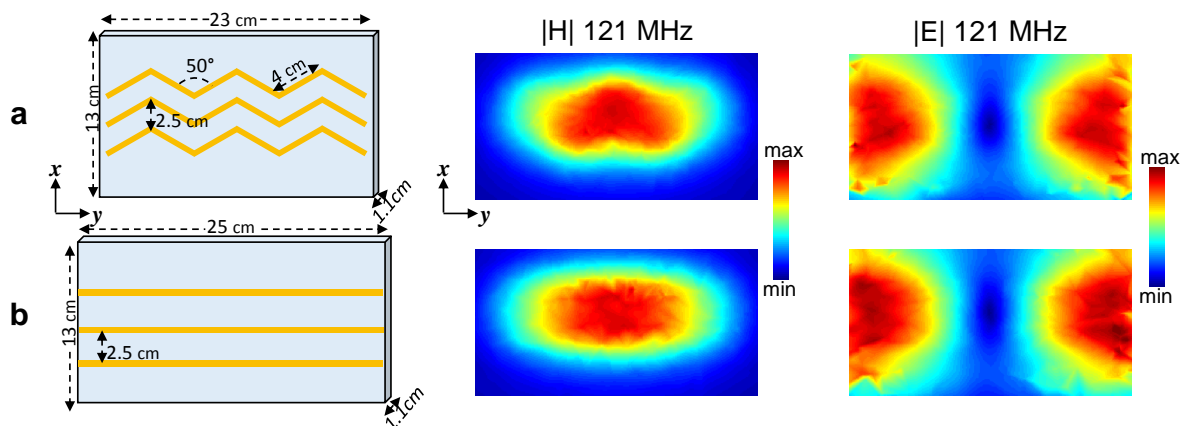
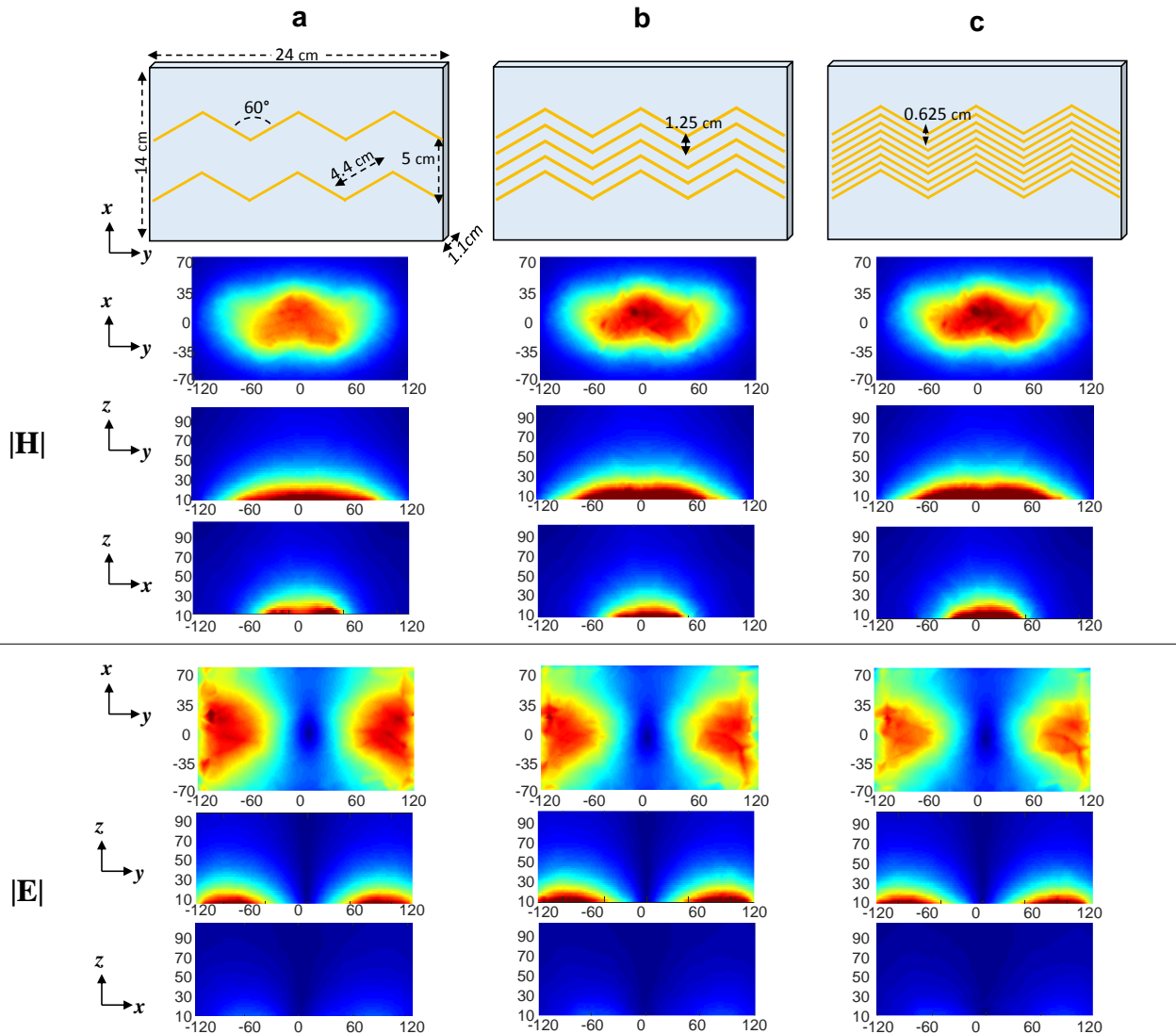


**Figure S1: Comparison of a zigzag-shaped versus straight-line strips metamaterials. a,** zigzag-shape three-strips structure for  $^{31}\text{P}$  frequency at 7 T (121 MHz) and **b,** equivalent

straight-line strips structure, Each case includes a schematic structure and its dimensions,  $|H|$  and  $|E|$  field distribution at 20 mm from the structure in  $XY$  plane.

## S2. Resonant mode dependence versus number of sub-units in a metasurface

An important topic requiring analysis concerns the effect of the number of unit cells within a metasurface on the structure of the resonant mode. In order to study the effect, we performed a series of simulations varying the number of strips. We performed this analysis for both the low frequency band using set of long strips and for the high frequency band using



a matrix of short strips. Figures S2.1 and S2.2 summarize the results, respectively.

**Figure S2.1: Low frequency band - comparison of H-field and E-field distribution as a function of the number of strips.** a, two strips at a separation of 5 cm, b, five strips at a separation of 1.25 cm and c, nine strips at a separation of 0.625 cm, keeping the total width the same. The frequencies of the mode corresponding to the setups are slightly shifted a) 121 MHz, b) 118 MHz and c) 114 MHz. The scaling is the same for all H-fields and E-fields, respectively.

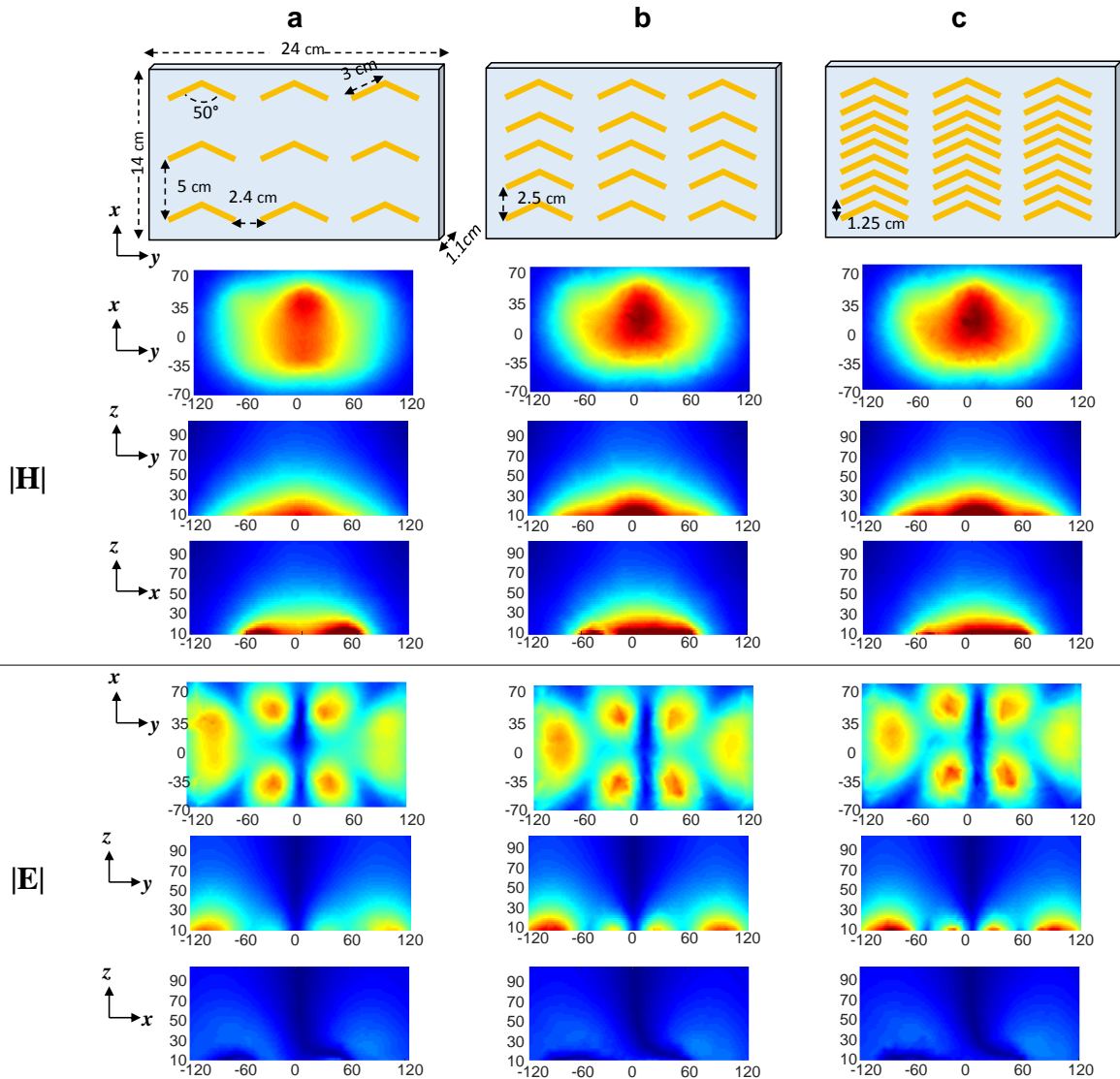


**Figure S2.2: High frequency band - comparison of H-field and E-field distribution as a function of the number of strips.** **a**, 9 strips (3x3 matrix) **b**, 15 strips (5x3 matrix) and **c**, 28 strips (9x3 matrix), keeping the total width constant. The frequencies of the mode corresponding to the setups are a) 298 MHz, b) 289 MHz, and c) 285 MHz. The scaling is the same for all H-fields and E-fields, respectively.

As can be seen, the resonant mode distribution is largely maintained irrespective of the number of strips, with small changes that observed mainly in close vicinity to the structure. Since in MRI usually one has a 1-2 cm distance from the coil structure to the imaging field-of-view, the effect is negligible.

Another point worth noting is the asymmetric distribution of the field. The local asymmetry includes local peaks, especially in the E-field and mainly in the resonant mode for the high frequency band. The origin of this asymmetry is the asymmetry of the in-plane

distribution of the strips, mainly caused by the length of the strips being greater than the separation between the strips. To overcome this asymmetry and obtaining more homogeneous distribution, one can utilize better packaging of the strips, as in an example demonstrated in the following figure.

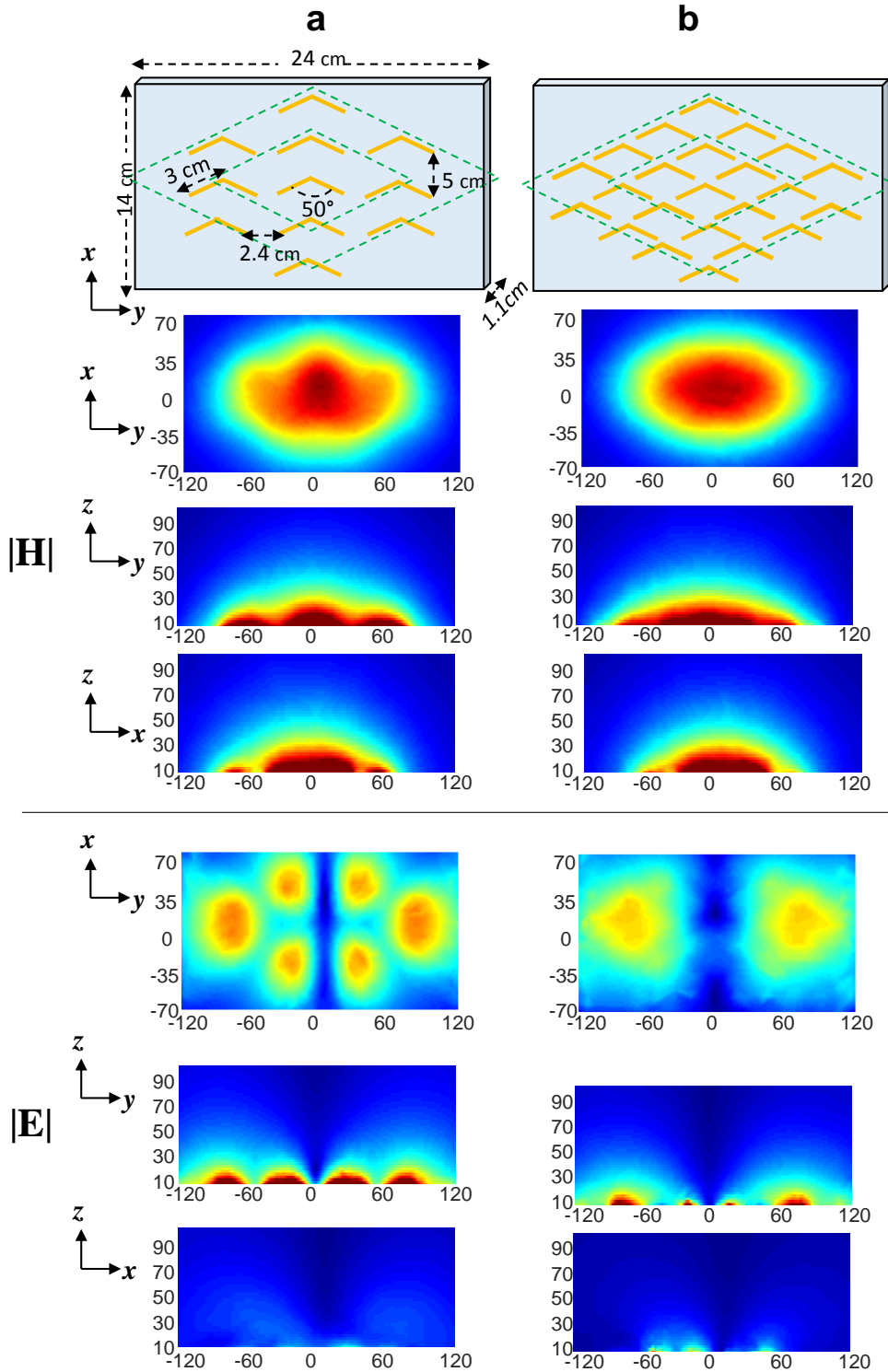


**Figure S2.3: High frequency band – realization of more homogeneous H-field and E-field distribution by more compact strips packaging. a, 11 strips and b, 23 strips with a rhombus-shaped packaging. The frequencies of the mode are shifted a) 298 MHz, b) 220 MHz. The scaling is the same for all H-fields and E-fields, respectively.**

### S3. Phantom $^{31}\text{P}/^1\text{H}$ dual-nuclei MRI verification

In this section, we examined the dual-nuclei metamaterial shown in **Figure 3a** in a phantom experiment. Figure S3 shows the  $^1\text{H}$  imaging and  $^{31}\text{P}$  spectroscopic imaging of a phantom with and without the metamaterial. The phosphorous phantom contained phosphoric acid ( $\text{H}_3\text{PO}_4$ ) having one  $^{31}\text{P}$  peak. The measured local enhancement, for the same excitation tip angle, was similar to the expected in the simulation, 1.9 for  $^{31}\text{P}$  and 2.1 for  $^1\text{H}$  (the noise was calculated as a standard deviation in a region placed outside the objects in the image).

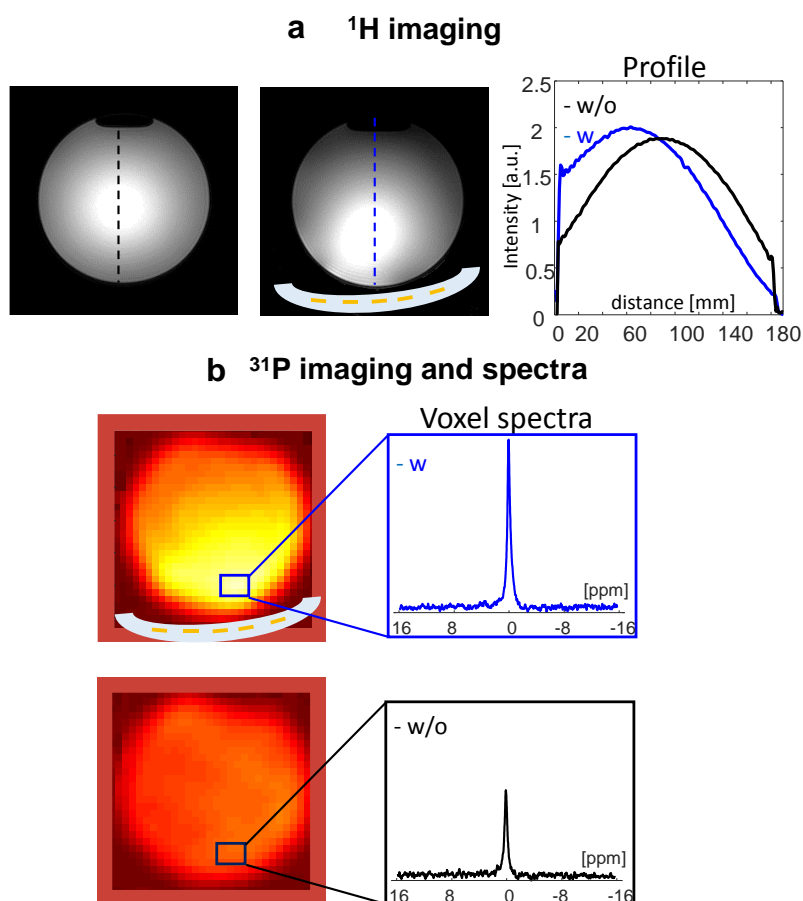


**Figure S3: Phantom experimental results.** **a**,  $^1\text{H}$  images without and with the metamaterial and the profile through the phantom as shown by the dashed line with maximum enhancement of 2.1 very close to the metamaterial. **b**,  $^{31}\text{P}$  images with and without the metamaterial, as well as a spectra of a voxel in the vicinity of the metamaterial with a maximum enhancement of 1.9 close to the metamaterial. The phosphorous phantom consists of phosphoric acid ( $\text{H}_3\text{PO}_4$ ) with one  $^{31}\text{P}$  peak. The position of the metamaterial below the phantom is shown.

#### S4. Sodium ( $^{23}\text{Na}$ ) and proton ( $^1\text{H}$ ) dual nuclei MRI metamaterial

In this section, we also examined a potential design for sodium and proton imaging (not covered in the main manuscript), which shows the possibilities of extending this approach to even lower RF frequencies (sodium's gyromagnetic ratio is 0.26 that of the proton). In this case, the overall length of 30 cm was used, and the thickness was kept as 1.1 cm. Figure S4 shows the schematic structure and dimensions, as well as the  $|H|$  fields for the  $^{23}\text{Na}$  and  $^1\text{H}$  frequency bands.

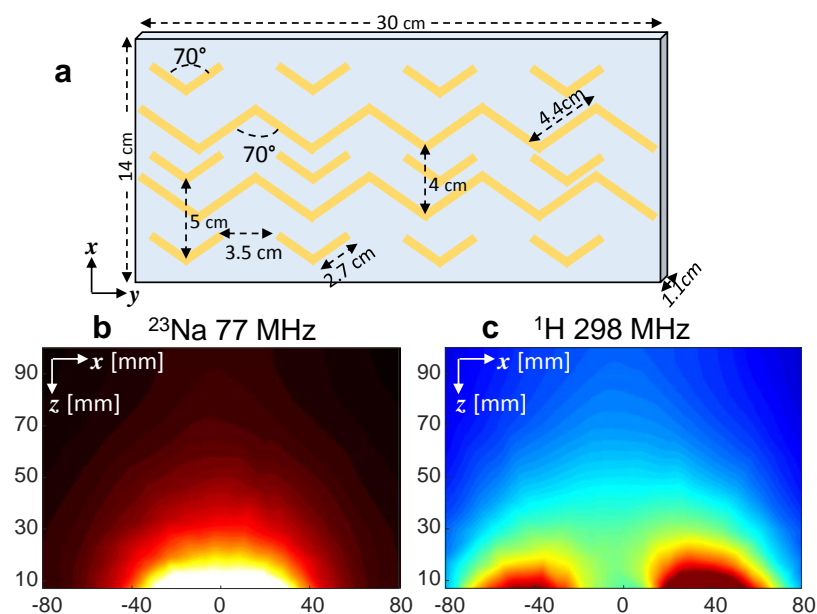


**Figure S4: Configurations of the  $^{23}\text{Na}$  /  $^1\text{H}$  dual-nuclei metamaterial.** **a**, A schematic of the structure and dimensions. **b,c** The central cross section in the XZ plane for the  $^{23}\text{Na}$  and  $^1\text{H}$  frequency bands, respectively. The  $^{23}\text{Na}$  maps are displayed with a “hot” color map and the  $^1\text{H}$  maps are displayed with a “jet” color map.